Chapter 5

Synthesis and Characterization of Ruthenium Intercalators with High Redox Potentials and Their Chemistry with DNA[‡]*

[‡]Synthetic work performed in collaboration with Dr. Alexander Schnyder

*EPR experiments performed by Dr. Jae Yoo

5.1 Introduction

Transition metal complexes of the type $[Ru(L)_2dppz]^{2+}$, (L = 2,2'-bipyridine (bpy) and 1,10-phenanthroline (phen)) are well-known DNA intercalators.[1] NMR[2] and time-resolved spectroscopic[3] studies indicate these complexes exhibit a slight sequence preference when binding to DNA, although nowhere near the magnitude required for the intercalators to bind in a site-specific manner. Structural studies have shown binding occurs via intercalation of the dppz ligand from the major groove side of the double helix, with a distribution of intercalation geometries being observed.[2]

The luminescence behavior of these dipyridophenazine-based metallointercalators is very sensitive to the solvent environment. In organic solutions, emission from the photoexcited Ru-dppz metal-to-ligand charge transfer (MLCT) state is easily detected. In aqueous and protic solutions, the emission is quenched via the interaction of protons with the phenazine nitrogens on the dppz ligand. After examining photoexcited $[Ru(L)_2dppz]^{2+}$, quenching by various proton donors in non-aqueous solutions, Turro and coworkers[4] concluded that the emission quenching was a result of proton transfer to a phenazine nitrogen on the dppz moiety. Olson et al.[5] have postulated that hydrogen bonding to the phenazine nitrogens opens up an intramolecular charge transfer pathway from the initial MLCT to a new MLCT species that decays in a non-radiative manner.

Clearly, the accessibility of the phenazine nitrogens on the dipyridophenazine ligand plays a crucial rule in determining the luminescent behavior of $[Ru(L)_2dppz]^{2+}$ complexes in a given system. In an aqueous, buffered solution containing double strand DNA, preferential intercalation of the dppz ligand into the double helix protects the phenazine nitrogens from the bulk solvent, allowing the metallointercalators to luminesce. This phenomenon, aptly referred to as a molecular "light switch" effect, makes these molecules very sensitive probes for double helical DNA.

Intercalation places these metal complexes in intimate contact with the DNA π stack. This should make them ideal reactants for chemistry with the DNA bases. Several

laboratories have observed oxidative damage to DNA with a wide range of reactants including photoexcited rhodium(III) intercalators,[6] anthraquinones,[7] and napthalamides.[8] Damage is observed primarily at guanine residues, in accordance with experiments[9] and theoretical predictions[10] that determined guanine is the most easily oxidized base. Similar chemistry with ruthenium-based intercalators was desirable, as they offer many advantages over the aforementioned systems including (1) longer excited-state lifetimes, (2) greater synthetic control of redox potentials, and (3) higher quantum yields for oxidative reactions. Indeed, it has been shown that *in situ* generated Ru(III) intercalators are capable of oxidizing guanine in a DNA double helix.[11] Remarkably, when the metallointercalators are tethered to the end of a DNA duplex, guanine oxidation may be induced up to 200 Å away.[12] DNA damage induced by these metallointercalators has also been observed in cells,[13] underscoring the importance of understanding charge migration through the DNA π stack.

In situ generation of the Ru(III) intercalators is achieved via the flash-quench technique which was originally developed to characterize charge transfer in proteins.[14] The scheme outlining the flash-quench series of reactions is illustrated in Figure 5.1. The cycle is initiated by visible light, typically at the MLCT wavelength of the Ru(II) complex. The excited-state Ru(II) is then quenched by a non-intercalating electron-accepting quencher (in these studies ruthenium(III) hexaammine) to form a Ru(III) intercalator *in situ*. The newly-generated ruthenium(III) intercalator is then able to react with the DNA (assuming it has enough driving force to do redox chemistry) until it leaves the double helix or is converted to ruthenium(II) by recombination (back electron transfer) with the reduced quencher. This technique has been used not only to generate oxidative damage at a distance in DNA duplexes, but also to spectroscopically (with both time-resolved transient absorption[15] and electron paramagnetic resonance)[16] observe the guanine radical within the DNA double helix.

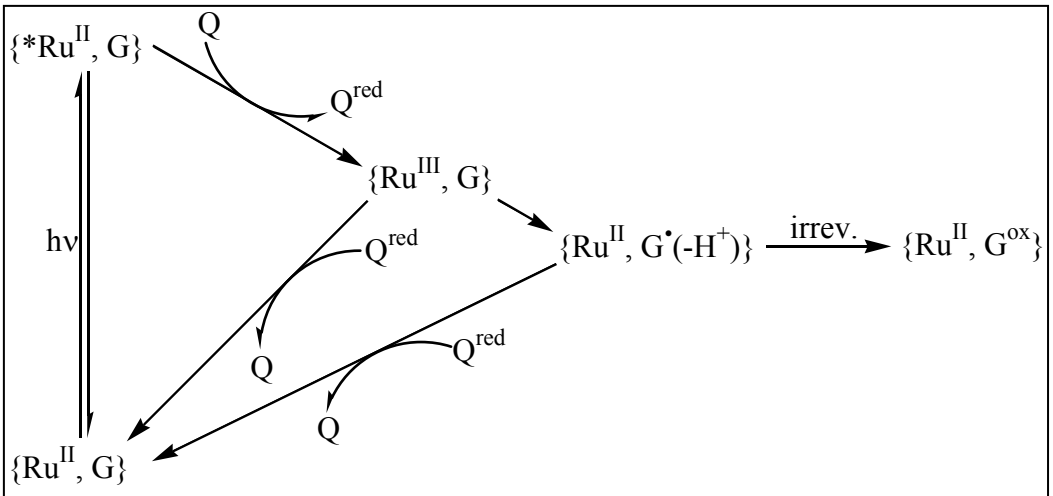

Figure 5.1 Flash-quench cycle for the oxidation of guanine by an *in situ* generated ground state ruthenium(III) species.

The ability to synthesize intercalators with a wide range of spectroscopic and electrochemical properties make dipyridophenazine-based ruthenium complexes ideal for studying the nuances of charge transfer through DNA. Previous studies in our laboratory have focused on synthesizing ruthenium intercalators with a variety of intercalating dppz-like ligands.[17] The photophysical properties of a series of osmium intercalators in which the ancillary (i.e., non-intercalating) ligands were varied have also been examined, although those metallointercalators did not have sufficient redox potentials to allow oxidative damage to DNA to be studied.[18]

The goal of these studies was to vary the architecture of the ancillary ligands to create ruthenium intercalators with high redox potentials (Figure 5.2). This chapter describes the synthesis and photophysical and electrochemical properties of several dppz-based ruthenium(II) intercalators containing ancillary bipyridine ligands that incorporate a variety of electron-withdrawing substituents. Theory predicts[19] that electron-withdrawing substituents placed at appropriate positions on bipyridine ligands should raise the 3+/2+ ruthenium (metal-centered) redox couple by a few hundred millivolts relative to the parent polypyridyl complex. Oxidation potentials in this range allow us to

study oxidative damage to purines in DNA duplexes. The monitoring of this damage by a variety of biochemical and spectroscopic methods is detailed.

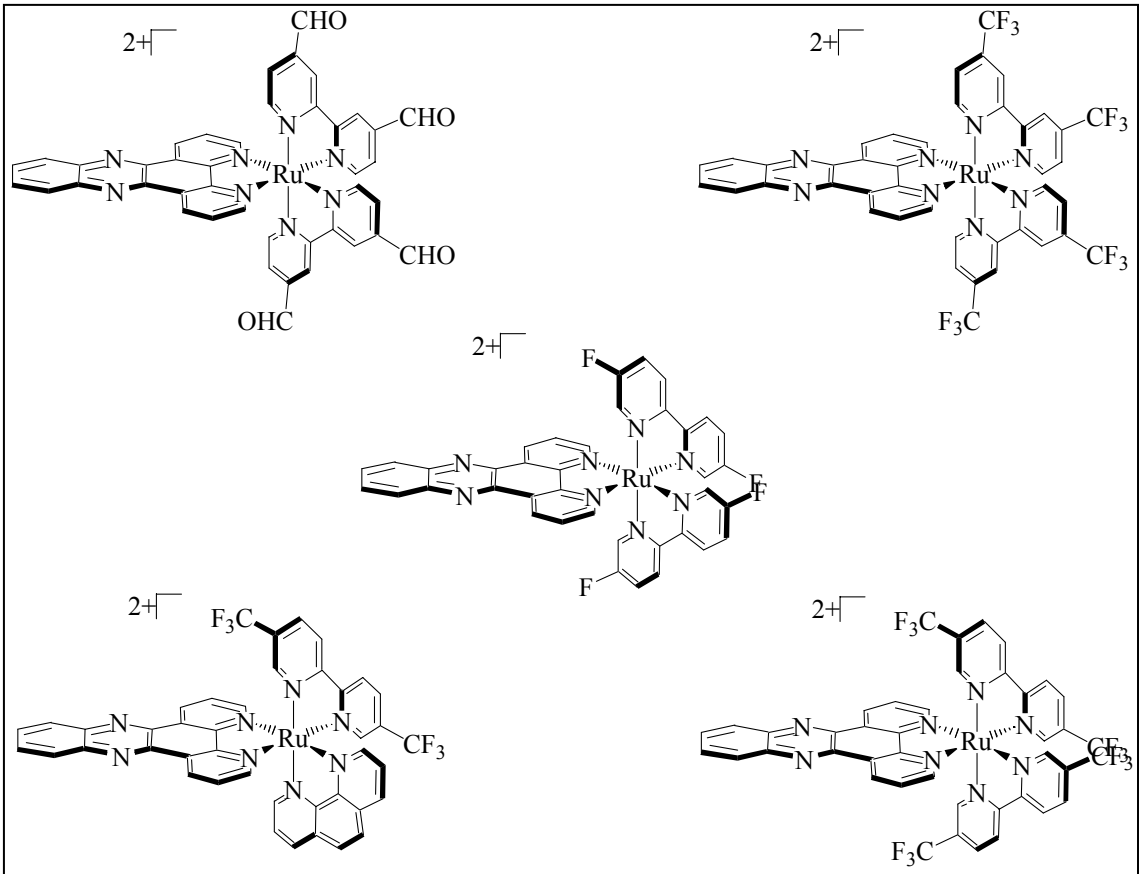

Figure 5.2 Structures of the various Ru(II)/dppz intercalators employed in these studies.

5.2 Experimental Section

Methods and Materials. Unless otherwise specified, commercial chemicals were purchased from Aldrich and used as supplied. QAE-A25 anion exchange resin was purchased from Aldrich. Dipyrido[3,2-a:2′,3′-c]phenazine (dppz),[20,21] 5,5′-bis(trifluoromethyl)-2,2′-bipyridine (5,5′-CF_3bpy),[22,23] 4,4′-bis(trifluoromethyl)-2,2′-bipyridine (4,4′-CF_3bpy),[22,23] and $[Ru(phen)_2dppz]Cl_2$,[24,25] were prepared according to

published procedures. Sonicated, phenol-extracted calf thymus DNA, poly d(AT), poly d(GC), and poly d(IC) were purchased from Pharmacia.

NMR spectra (^{1}H and ^{19}F NMR) were taken on a General Electric QE PLUS 300 MHz instrument using solvent as the internal standard. UV-visible spectra were measured on a Varian Cary 2200, a Hewlett Packard HP8452A, or a Beckmann DU 7400 UV/VIS spectrophotometer. High performance liquid chromatography (HPLC) of the various metal complexes was performed on a Hewlett-Packard 1050 HPLC (100–50% NH_4OAc, 0–50% CH_3CN over 50 minutes, Rainin C4 Dynamax column).

Syntheses and Characterization. [Ru(phen)(5,5′-CF_3bpy)(dppz)]Cl_2. $[Ru(CO)_2(phen)(OTf)_2]$ (100 mg, 0.16 mmol), prepared according to literature procedures,[26–28] was dissolved in 2 mL of 2-methoxyethanol at ambient temperature and flushed with nitrogen. 5,5′-CF_3bpy (55 mg, 0.19 mmol) was added to the solution and refluxed for 2 hours. The yellow suspension was then cooled to room temperature, and a saturated aqueous solution of NH_4PF_6 was added to the mixture. The light yellow $[Ru(CO)_2(phen)(5,5′\text{-}CF_3bpy)]^{2+}$ complex was precipitated as the PF_6^- salt, filtered, and washed with copious amounts of water and dried with diethyl ether. The crude product (50 mg, 0.05 mmol) was dissolved in 4 mL of 2-methoxyethanol and flushed with nitrogen for 30 minutes. To the solution was added dppz (32 mg, 0.11 mmol) and trimethylamine-N-oxide (18 mg, 0.16 mmol). The mixture was heated at reflux for 1.5 hours forming a dark orange solution. The crude reaction mixture was purified on an alumina column using a shallow water/acetonitrile gradient (increase by 1% water/100 mL mobile phase) and exchanged to the chloride salt on a Sephadex QAE-A25 anion exchange column. The fractions containing the complex were concentrated, dissolved in methanol, and the product was precipitated as orange crystals by adding diethyl ether. Yield (Cl^- salt): 39 mg (34%). ^{1}H NMR (Acetone-d_6, 300 MHz): δ 9.71 (dd, 2H), 9.26 (dd, 2H), 8.86 (dd, 1H), 8.82 (d, 2H), 8.70 (dd, 1H), 8.61 (m, 3H), 8.55–8.36 (m, 7H), 8.21 (m, 2H), 8.12 (m, 1H), 7.96 (m, 2H), 7.78 (dd, 1H). ^{19}F NMR (Acetone-d_6, 300

MHz): δ -64.3 (s, 3F), -64.4 (d, 3F). MS (MALDI-TOF, Cl^- salt): *m/z* calculated for $C_{42}H_{24}N_8F_6Ru$ ($[M-2Cl]^+$) 855.79, found 855.70; *m/z* calculated for $C_{30}H_{18}N_6Ru$ ([M-2Cl-(5,5'-CF_3bpy)]$^+$) 563.58, found 563.90.

5,5′-difluoro-2,2′-bipyridine (5,5′-F_2bpy). To a 100 mL three necked flask were added a magnetic stir bar, a gas inlet adaptor, a rubber septum, $Ni(Br)_2(PPh)_2$ (1.898 g, 2.55 mmol), zinc powder (0.808 g, 12.42 mmol), and Et_4NI (1.664 g, 8.28 mmol) under nitrogen pressure. Dry and O_2-free THF (20 mL) was added by syringe through a septum. The reaction mixture was stirred at room temperature for 30 min., changing color to a dark red solution. 2-Chloro-5-fluoropyridine[29] (1.08 g, 8.28 mmol) in 5 mL dry THF was added via syringe and the solution was heated at 40 ^oC for 1.5 hours. The reaction mixture was poured into 2 M aqueous ammonia (75 mL), and precipitates were filtered off. The filtrate was extracted 4 times with $CHCl_3$ (200 mL). The organic layer was washed with water , dried with $MgSO_4$, and evaporated under reduced pressure. The residue was chromatographed on silica gel using CH_2Cl_2 as an eluant to give 5,5′-difluoro-2,2′-bipyridine. Yield: 365 mg (46%). ^1H NMR (CD_3OD, 300 MHz): δ 8.49 (d, 2H), 8.37 (dd, 2H), 7.51 (m, 2H). ^{13}C NMR (CD_3OD, 300 MHz): δ 137.5 (d, 2C), 123.8 (d, 2C), 122.2 (d, 2C), 8.30 (dd, 2H). MS (ESI): *m/z* calculated for $C_{10}H_7N_2F_2$ ($[M+H]^+$) 193.18, found 193.13; *m/z* calculated for $C_{10}H_6N_2$ ($[M-2F]^+$) 154.17, found 154.11.

[Ru(5,5′-F_2bpy)$_2$dppz]Cl_2. $RuCl_3$•$3H_2O$ (67 mg, 0.26 mmol), 5,5′-difluoro-2,2′-bipyridine (100 mg, 0.52 mmol) and LiCl (111 mg, 2.61 mmol) were suspended in DMF (3 mL) and heated at reflux for 12 hours. The reaction mixture turned dark over the course of the reaction. The reaction mixture was cooled to room temperature, then 5 mL of acetone and 5 mL of diethyl ether were added. A dark blue precipitate [Ru(5,5′-F_2bpy)Cl_2]•$2H_2O$ (215 mg) was collected after cooling over night at –20 ^oC and washed thoroughly with ethanol. The crude Ru complex (50 mg) and dipyrido[3,2-a:2′,3′-c]phenazine (20 mg) were dissolved in 5 mL of ethylene glycol and refluxed for 2 hours.

The color of the mixture changed from dark blue to dark red. After cooling to room temperature, an aqueous solution of NH_4PF_6 was added, causing the PF_6^- salt of the product to precipitate. The suspension was filtered and washed thoroughly with copious amounts of water and diethyl ether. The counterion was exchanged to chloride on a Sephadex QAE-A25 anion exchange column (resin equilibrated with 0.2 M KCl solution) and purified on an alumina column using a shallow water/acetonitrile gradient (increase by 1% water/100 mL mobile phase). The fractions containing the complex were concentrated, dissolved in methanol, and the product was precipitated as an orange solid by adding diethyl ether. Yield (Cl^- salt): 25 mg (12%). ^{1}H NMR (CD_3OD, 300 MHz): δ 9.81 (d, 2H,), 8.81 (m, 4H), 8.49 (m, 4H), 8.30 (dd, 2H), 8.12 (m, 4H), 8.01 (m, 6H), 7.93 (m, 1H), 7.72 (m, 1H). ^{19}F NMR (CD_3OD, 300 MHz): δ -119,3 (s, 2F), -119, 6 (s, 2F). MS (MALDI-TOF, Cl^- salt): *m/z* calculated for $C_{38}H_{22}N_8F_3ClRu$ ($[M\text{-}Cl\text{-}F]^+$) 784.16, found 782.70; *m/z* calculated for $C_{38}H_{22}N_8F_4Ru$ ($[M\text{-}2Cl]^+$) 767.71, found 767.80; *m/z* calculated for $C_{38}H_{22}N_8F_4Ru$ ($[M\text{-}2Cl\text{-}(5,5'\text{-}F_2bpy)]^+$) 575.54, found 575.80.

[Ru(4,4′-CHObpy)$_2$dppz]Cl$_2$. $RuCl_3 \bullet 3H_2O$ (140 mg, 0.54 mmol), 2,2′-bipyridine-4,4′-dicarboxaldehyde (250 mg, 1.18 mmol) and LiCl (244 mg, 5.3 mmol) were suspended in DMF (5 mL) and heated at reflux for 12 hours. The reaction mixture changed color to a purple solution. The reaction mixture was cooled to room temperature, then 5 mL of acetone and 10 mL of diethyl ether were added. A dark blue precipitate $[Ru(4,4'\text{-}CHObpy)_2Cl_2] \bullet 2H_2O$ (215 mg) crashed out of the reaction mixture immediately and was collected and washed thoroughly with ethanol. The crude Ru(II) complex and dipyrido[3,2-a:2′,3′-c]phenazine (22 mg) were dissolved in 2 mL of ethylene glycol and refluxed for 2 hours. The color of the mixture changed from dark blue to a dark orange solution. After cooling to room temperature the crude solution was washed with de-ionized water through a Sep-Pak cartridge to separate the complex from ethylene glycol. The product was washed out of the column with a mixture of acetonitrile and a 0.1% trifluoroacetic acid in water solution (9:1) and rotavapped to

dryness. The crude orange Ru(II) complex was purified on an alumina column using a shallow water/acetonitrile gradient (increase by 1% water/100 mL mobile phase). The fractions containing the complex were concentrated, dissolved in methanol, and the product was precipitated as an orange solid by adding diethyl ether. Yield (Cl^- salt): 54 mg (11%). ^{1}H NMR (CD_3OD, 300 MHz): δ 8.65 (m, 4H), 8.39 (m, 4H), 8.16 (m, 2H), 8.03 (m, 2H), 7.94–7.71 (m, 10H), 7.75 (m, 2H), 7.36 (m, 2H). MS (MALDI-TOF, Cl^- salt): *m/z* calculated for $C_{42}H_{26}N_8ClO_4Ru$ ($[M-Cl]^+$) 843.2, found 842.1; *m/z* calculated for $C_{42}H_{26}N_8O_4Ru$ ($[M-2Cl]^+$) 807.79, found 809.9; *m/z* calculated for $C_{30}H_{18}N_6O_2Ru$ ($[M-2Cl-(4,4'-CHObpy)]^+$) 594.6, found 595.0.

[Ru(5,5′-CF_3bpy)$_2$dppz](PF$_6$)$_2$. 80 mg (0.28 mmol) of dppz were dissolved in 10 mL of ethylene glycol at 150 °C. Crude $[Ru(5,5'CF_3bpy)_2Cl_2]\bullet 2H_2O$ (185 mg, 0.23 mmol) was then added, causing the reaction mixture to turn dark purple. After 30 minutes, the reaction color became dark red. Heating was continued for an additional 30 minutes followed by cooling to room temperature. The reaction mixture was then diluted to 100 mL with Milli-Q H_2O. Excess solid NH_4PF_6 was added, causing an orange precipitate to form which was isolated on a medium porosity filter frit and washed with 75 mL of H_2O followed by 75 mL of diethyl ether. This solid was then dissolved in a minimal amount of a CH_3CN/CH_2Cl_2 mixture and chromatographed on a neutral alumina column using CH_3CN as the eluant. The desired red-colored fraction was rotovapped to dryness, dissolved in a minimal amount of CH_3OH, precipitated as an orange solid by the addition of excess diethyl ether, isolated on a medium porosity filter frit, and dried overnight in a vacuum dessicator. Yield (PF_6^- salt): 176 mg (60%). ^{1}H NMR (CD_3CN, 300 MHz): δ 9.72 (dd, 2H), 8.81 (m, 4H), 8.49 (m, 4H), 8.37 (m, 2H), 8.13 (m, 4H), 8.05 (m, 2H), 7.91 (m, 4H). MS (FAB, PF_6^- salt): *m/z* calculated for $C_{42}H_{22}N_8F_{18}PRu$ ($[M-PF_6]^+$) 1113.05, found 1113.08; *m/z* calculated for $C_{42}H_{22}N_8F_{18}PRu$ ($[M-2PF_6]^+$) 968.08, found 968.09.

[Ru(4,4′-CF_3bpy)$_2$dppz](PF_6*)$_2$.* 39 mg (0.14 mmol) of dppz were dissolved in 10 mL of ethylene glycol at 150 °C. Crude [Ru(4,4′-CF_3bpy)$_2Cl_2$] •$2H_2O$ (91 mg, 0.12 mmol) were then added, causing the reaction mixture to turn dark purple. After 1 hour, 65 mg (0.27 mmol) of silver triflate were added and the solution became dark red. Heating was continued for an additional 60 minutes followed by cooling to room temperature. The reaction mixture was then diluted to 50 mL with Milli-Q H_2O. Excess solid NH_4PF_6 was added, causing a dark orange precipitate to form which was isolated on a medium porosity filter frit and washed with 75 mL of H_2O followed by 75 mL of diethyl ether. This solid was then dissolved in a minimal amount of a CH_3CN/CH_2Cl_2 mixture and chromatographed on a neutral alumina column using CH_3CN as the eluant. The desired red-colored fraction was rotovapped to dryness, dissolved in a minimal amount of CH_3OH, precipitated as an orange solid by the addition of excess diethyl ether, isolated on a medium porosity filter frit, and dried overnight in a vacuum dessicator. Yield (PF_6^- salt): 29 mg (20%). ^{1}H NMR (CD_3CN, 300 MHz): δ 9.76 (m, 2H), 9.01 (m, 4H), 8.51 (m, 4H), 8.16 (m, 4H), 7.97 (m, 4H), 7.76 (m, 2H), 7.57 (m, 2H). MS (FAB, PF_6^- salt): *m/z* calcd. for $C_{46}H_{28}N_8O_4F_{12}Ru$ ($[M]^+$) 1069.6; found 1072.6.

Sample Preparation. All oligonucleotides were purified by reverse phase HPLC (0–15% CH_3CN over 35 minutes, C18 Dynamax column) and de-salted prior to use. Oligonucleotide duplexes were created by hybridizing the appropriate amounts of complementary single strands based on calculated extinction coefficients for unmodified sequences (ε_{260} ($M^{-1}cm^{-1}$): dC = 7400; dT = 8700; dG = 11,500; dA = 15,400.[30,31] Polymeric DNA was exchanged into a buffer of 5 mM NaPi, 50 mM NaCl, pH=7 via centrifugation (Amicon) and quantitated based on nucleotide concentration using the following extinction coefficients (ε_{260} ($M^{-1}cm^{-1}$): poly d(AT) = 6600; poly d(GC) = 8400; poly d(IC) = 6900; calf thymus DNA = 6600.

UV-visible Spectroscopy. The UV-visible spectra for all complexes were taken in H_2O. For titrations with calf thymus DNA, a 10 μM solution of racemic metal complex

was measured in buffer. To this was added small aliquots of a concentrated calf thymus DNA stock solution (ca. 18 mM) in increments up to Ru:base pair = 1:50. Extinction coefficients for complexes were obtained as follows: accurate measurements of ruthenium concentrations were made using a Perkin-Elmer/Sciex Elan 5000A ICP-MS and $[Ru(bpy)_3]Cl_2$ as a calibrant, and absorbance measurements of the samples were obtained on a Hewlett Packard HP8452A spectrophotometer. A standard curve was generated with the $[Ru(bpy)_3]Cl_2$ samples, and the extinction coefficients of the complexes were determined using this curve.

Electrochemistry. Ground-state oxidation and reduction potentials for the ruthenium complexes were obtained on a Bioanalytical Systems (BAS) model CV-50W electrochemical analyzer. A glassy carbon working electrode, Ag/AgCl reference electrode, and Pt auxiliary electrode were used in a single cell sample apparatus. Solutions of racemic metal complex (1 mM, PF_6^- salts) in dry acetonitrile (Fluka, stored over molecular sieves) containing 100 mM tetrabutylammonium hexafluorophosphate (Aldrich) were degassed with argon prior to use. Voltammograms were collected using a 100 mV/s scan rate. $E_{1/2}$ values were taken as the average of the voltage of maximum current for the forward and reverse electrochemical processes. Potentials are reported in volts versus NHE.

Steady-state Spectroscopy. All metal complexes were purified via HPLC and de-salted prior to use. Emission and excitation spectra were obtained on an ISS K2 spectrofluorometer. Emission intensities were determined by integration of the luminescence spectrum and standardized against $[Ru(bpy)_3]Cl_2$ as a calibration for the instrument. Solutions containing 10 μM racemic metal complex (OAc^- salt) were excited at their MLCT maximum, and emission was monitored from 500–800 nm. Excitation spectra were obtained by monitoring at the emission maximum while varying excitation wavelength from 350–600 nm.

Time-resolved Spectroscopy. All metal complexes were purified via HPLC and de-salted prior to use. Time-resolved transient absorption and fluorescence measurements were conducted using a pulsed YAG-OPO laser (λ_{exc} = 470 nm). Laser powers ranged from 2 to 4 mJ/pulse. The ruthenium concentration (racemic, OAc^- salt) in all samples was 20 μM. The buffer used in both fluorescence and transient absorption measurements was 5 mM NaPi, 50 mM NaCl, pH=7. Calf thymus DNA (0.8 mM nucleotides) was used in determining lifetimes of the racemic metal complexes with DNA. In the transient absorption experiments of metal complexes bound to DNA, 0.8 mM nucleotides of calf thymus DNA and 0.4 mM $Ru(NH_3)_6^{3+}$ were present.

Assay of Oxidative DNA Damage. Single DNA oligonucleotides containing a guanine doublet site were 5'-^{32}P end-labeled and annealed to the complementary strand in a buffer of 5 mM sodium phosphate, 50 mM NaCl, pH 7. Oligonucleotide duplexes (8 μM) containing 16 μM racemic metal complex, and 160 μM $Ru(NH_3)_6^{3+}$ as an oxidative quencher were irradiated at 450 nm with a 1000 W Hg/Xe lamp equipped with a monochromator. Irradiation times were varied from 0 minutes to 30 minutes. After irradiation, samples were treated with 10% piperidine at 90 °C for 30 minutes, dried, and electrophoresed through a 20% denaturing polyacrylamide gel. Damage patterns were obtained by visualizing the gel via phosphorimagery.

EPR. EPR spectra were recorded using an X-band Bruker EMX spectrometer equipped with a standard TE_{102} cavity. Magnetic field calibrations were made against a degassed solution of 1% perylene in H_2SO_4. All measurements were made on photolyzed frozen solutions at 77 K. The temperature was maintained by employing a finger dewar filled with liquid nitrogen designed to fit inside the EPR cavity. All samples contained 0.8 mM DNA nucleotides, 20 μM Ru complex, and 400 μM $[Co(NH_3)_5Cl]Cl_2$ in a 10 mM KPi, 10 mM NaCl, pH=7.0 buffer. Photolysis was carried out by illuminating a 100 μL sample solution contained in quartz tubes (4mm OD) while being frozen in an optical dewar filled with liquid nitrogen. The samples were immediately frozen as irradiated.

The light source used was a 300 W Xe-Arc lamp (Varian Eimac Division, Light R300-3) powered by an Illuminator Power Supply (Varian Eimac Division, Model PS 300-1). UV filters were employed to eliminate light < 320 nm and water to eliminate IR radiation.

5.3 Results

Figure 1 (*vide supra*) illustrates the five dppz-based ruthenium(II) intercalators employed for these studies. Each metal complex contains at least one 2,2'-bipyridine which has been modified with electron-withdrawing substituents (CF_3, F, or CHO) at the 4 and 4' or 5 and 5' positions. Introduction of these substituents offers the possibility of tuning the optical and redox properties of the metallointercalator. This could be useful as we seek out new intercalators to probe DNA structure and reactivity.

5.3.1 UV-visible spectroscopy

Dipyridophenazine complexes of ruthenium(II) are characterized by intense absorption in the metal-to-ligand charge transfer (MLCT) excited states in the visible region of the electromagnetic spectrum.[1] Figure 5.3 shows the UV-visible spectrum of $[Ru(5,5'\text{-}CF_3bpy)_2dppz]^{2+}$ in water. This spectrum is representative of the others for the family of complexes presented in these studies. Peak positions and extinction coefficients are listed in Table 5.1. The broad peak in the 400–500 nm region is readily assigned to an MLCT state. The band in the 350–370 nm region arises from the π- π^* absorption of dppz.[25] The π- π^* transition of the bipyridine ligands, which is located in the upper 200 nm region, has a large absorbance whose energy varies slightly with the electron-withdrawing ability of the bpy ligands. Overall, the spectral features are what we would expect for $[Ru(L)_2dppz]^{2+}$-type complexes.

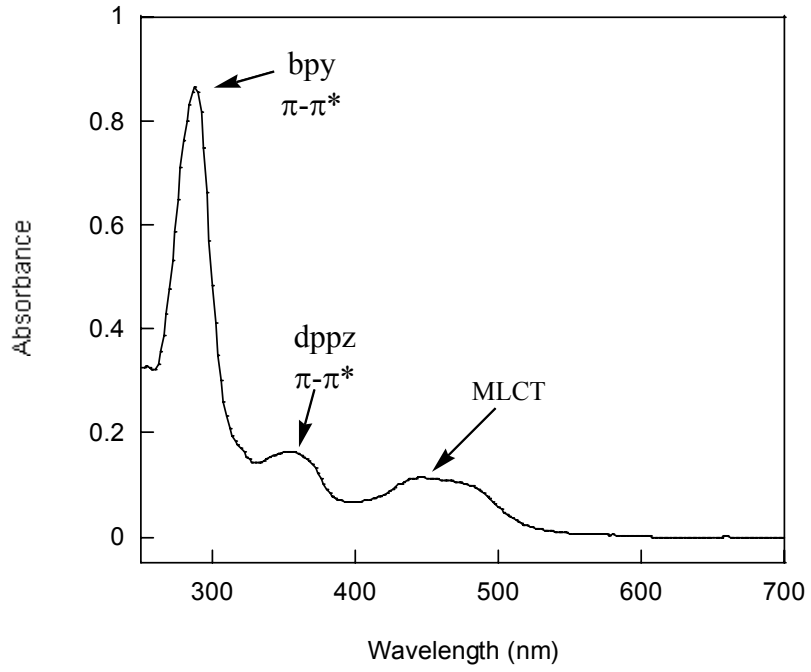

Figure 5.3 UV-visible spectrum of $[Ru(5,5'\text{-}CF_3bpy)_2dppz]^{2+}$ in water. The three types of absorption bands labeled in the Figure appear in all the metal complexes used in these studies. Peak positions and extinction coefficients for the various intercalators are given in Table 5.1.

	λ_{max} nm (ε x 10^{-3})		
Intercalator	MLCT	dppz π-π*	bpy π-π*
$[Ru(4,4'\text{-}CF_3bpy)_2dppz]^{2+}$	452 (21.3)	352 (28.6)	294 (113)
$[Ru(5,5'\text{-}CF_3bpy)_2dppz]^{2+}$	446 (13.4)	352 (19.3)	288 (102)
$[Ru(5,5'\text{-}F_2bpy)_2dppz]^{2+}$	430 (17.9)	356 (26.1)	280 (86.0)
$[Ru(4,4'\text{-}CHObpy)_2dppz]^{2+}$	458 (19.1)	356 (21.5)	280 (80.7)
$[Ru(5,5'\text{-}CF_3bpy)(phen)dppz]^{2+}$	430 (13.0)	368 (21.1)	280 (80.1) 264 (73.0)

Table 5.1 UV-visibile spectra parameters for the various intercalators in H_2O.

5.3.2 Redox properties

The introduction of electron-withdrawing substituents on the ancillary bpy ligands dramatically alters the electronic properties of the metal complexes. In general, the more electron-withdrawing ability the ancillary bipyridine ligands possess, the higher the oxidation potential. The reversible oxidation wave for the complexes at high positive potentials, corresponding to the Ru(III)/Ru(II) couple, ranges from 1.66 V – 1.84 V vs. NHE (see Table 5.2). These values are up to 0.2 V above those observed for unmodified dppz-based Ru(II) polypyridyl complexes and consistent with the electron-withdrawing substituents lowering the absolute energy of the highest occupied molecular orbital (HOMO) of the metal center.[32] It is readily apparent from the potentials that the +3 oxidation state of the metal complexes is capable of reacting with guanines in DNA.

The electrochemical reduction of these complexes is ligand-based and, unfortunately, not well resolved under the chosen experimental conditions. Those values

are reported in Table 5.2 as well. Nevertheless, it is easy to see that they occur at potentials near the typical values for polypyridyl ligands. Also shown in Table 5.2 are the E(0/0) values (energy at the intersection of the normalized absorption and fluorescence spectra) for each of the complexes. These allow the calculation of excited-state oxidation and reduction potentials, which are also shown in Table 5.2. The data suggest the excited state of the metal complexes might be able to react with guanines in DNA.

Intercalator	E(0/0)	E(3+/2+)	E(3+/*2+)	E(2+/1+)	E(*2+/1+)
$[Ru(4,4'\text{-}CF_3bpy)_2dppz]^{2+}$	2.16 V	1.80 V	-0.36 V	-0.75 V	1.41 V
$[Ru(5,5'\text{-}CF_3bpy)_2dppz]^{2+}$	2.12 V	1.84 V	-0.28 V	-0.57 V	1.55 V
$[Ru(5,5'\text{-}F_2bpy)_2dppz]^{2+}$	2.32 V	1.66 V	-0.66 V	-0.75 V	1.57 V
$[Ru(4,4'\text{-}CHObpy)_2dppz]^{2+}$	2.16 V	1.74 V	-0.42 V	-0.71 V	1.45 V
$[Ru(5,5'\text{-}CF_3bpy)(phen)dppz]^{2+}$	2.24 V	1.70 V	-0.54 V	-0.67 V	1.57 V

Table 5.2 Electrochemical parameters (vs. NHE) for the various ruthenium(II) intercalators determined in dry CH_3CN with 0.1 M $(Bu_4N)(PF_6)$ and a 100 mV/s scan rate. Oxidation peaks are reversible and reduction peaks are quasi-reversible. E(0/0) value taken as the point of intersection (after normalization) of the absorption and emission spectra in CH_3CN.

5.3.3 Spectroscopic properties in the absence and presence of DNA

UV-visible Spectroscopy. The well-resolved π- π* transition of the dppz ligand on the metal complexes provides an easy way to assay properties localized on this ligand, such as intercalation into the DNA helix. Addition of calf thymus DNA results in a slight red shift and hypochromism as the dppz moiety intercalates into the DNA base stack.[33]

An example of this phenomenon is shown in Figure 5.4 for $[Ru(5,5'\text{-}CF_3bpy)_2dppz]^{2+}$. The hypochromism values associated with intercalation of the dppz π- π* transitions of the various metallointercalators are listed in Table 5.3. They range from 11–29%. The lower end of that range represents complexes that do not intercalate deeply within the DNA double helix,[17] something quite unusual for dppz complexes. Unfavorable steric interactions between the bipyridine substituents and the DNA sugar-phosphate backbone can explain the results. These interactions would inhibit the dppz ligand from gaining intimate access to the DNA base stack, certainly affecting spectral and (possibly) redox properties of the compounds when bound to DNA.

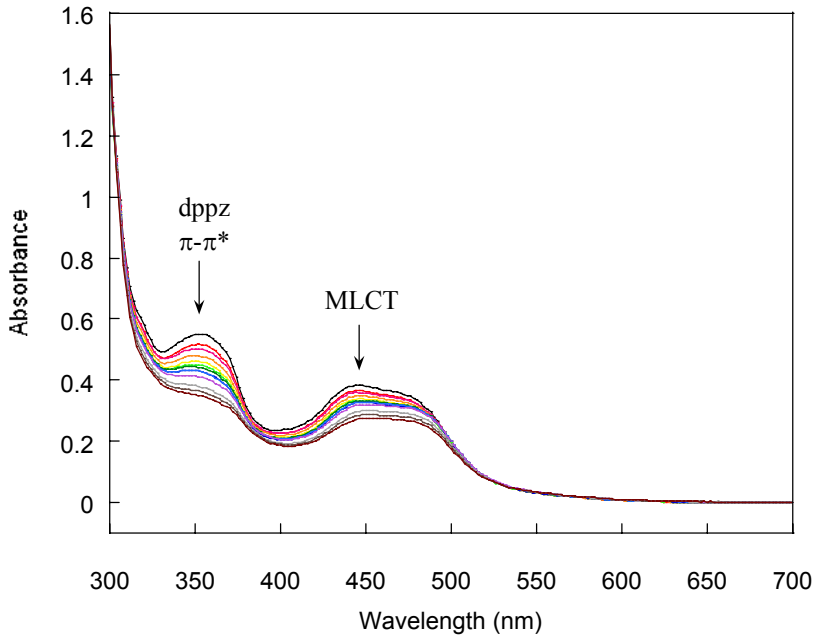

Figure 5.4 UV-visible titration of 10 μM $[Ru(5,5'\text{-}CF_3bpy)_2dppz]^{2+}$ with calf thymus DNA in 5 mM NaPi, 50 mM NaCl, pH=7. DNA concentration varied from 0–1 mM. Spectrum is representative of titrations for each of the metal complexes. Maximum % hypochromism upon intercalation for the dppz π-π* band is given in Table 5.3.

Intercalator	dppz π-π*	% Hypochromism
$[Ru(4,4'\text{-}CF_3bpy)_2dppz]^{2+}$	352 nm	26%
$[Ru(5,5'\text{-}CF_3bpy)_2dppz]^{2+}$	352 nm	17%
$[Ru(5,5'\text{-}F_2bpy)_2dppz]^{2+}$	356 nm	11%
$[Ru(4,4'\text{-}CHObpy)_2dppz]^{2+}$	356 nm	29%
$[Ru(5,5'\text{-}CF_3bpy)(phen)dppz]^{2+}$	368 nm	22%

Table 5.3 Maximum hypochromism associated with intercalation into calf thymus DNA measured at the dppz π-π* band for the various complexes. Experiments performed in 5 mM NaPi, 50 mM NaCl, pH=7. % hypochromism values recorded at 10 μM metal complex and 1 mM calf thymus DNA.

Luminescence Spectra. Excitation of Ru(II) polypyridyl complexes at their MLCT wavelengths typically leads to visible light emission from the ruthenium excited-state. Shown in Figures 5.5–5.9 are the fluorescence spectra for the complexes in acetonitrile, aqueous buffer, and DNA after excitation at their respective MLCT maximum. Quantum yields and wavelength parameters derived from the spectra are listed in Table 5.4.

Luminescence Properties in CH_3CN. The fluorescence spectral properties for the series of complexes in acetonitrile are summarized in Table 5.4. It is apparent that bipyridines substituted at the 4 and 4' positions give rise higher quantum yields than those substituted at the 5 and 5' positions. This is in agreement with previous studies examining the effects of electron-withdrawing substituents on bpy ligands[23] and is believed to be related to the energy gap law as applied to Ru(II) polypyridyl complexes (i.e., the position of electron-withdrawing groups at the 5 and 5' positions lowers the

energy of the emitting state, causing it to couple more strongly with the ground state and have a larger non-radiative rate constant).[34]

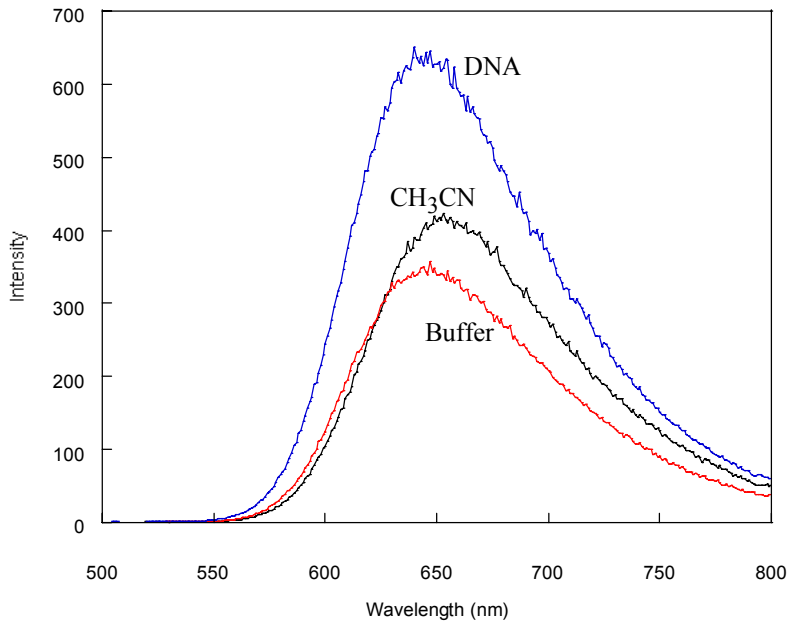

Figure 5.5 Fluorescence spectra of 10 μM $[Ru(4,4'\text{-}CF_3bpy)_2dppz]^{2+}$ in the presence of acetonitrile, buffer of 5 mM NaPi, 50 mM NaCl, pH=7, and 1 mM calf thymus DNA. Excitation at 452 nm. Peak positions and quantum yields are listed in Table 5.4.

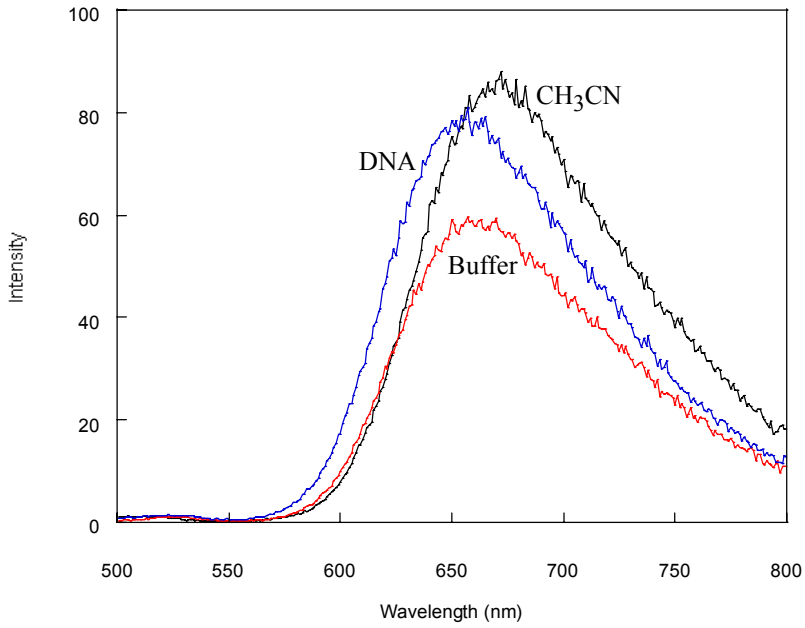

Figure 5.6 Fluorescence spectra of 10 μM $[Ru(5,5'\text{-}CF_3bpy)_2dppz]^{2+}$ in the presence of acetonitrile, buffer of 5 mM NaPi, 50 mM NaCl, pH=7, and 1 mM calf thymus DNA. Excitation at 446 nm. Peak positions and quantum yields are listed in Table 5.4.

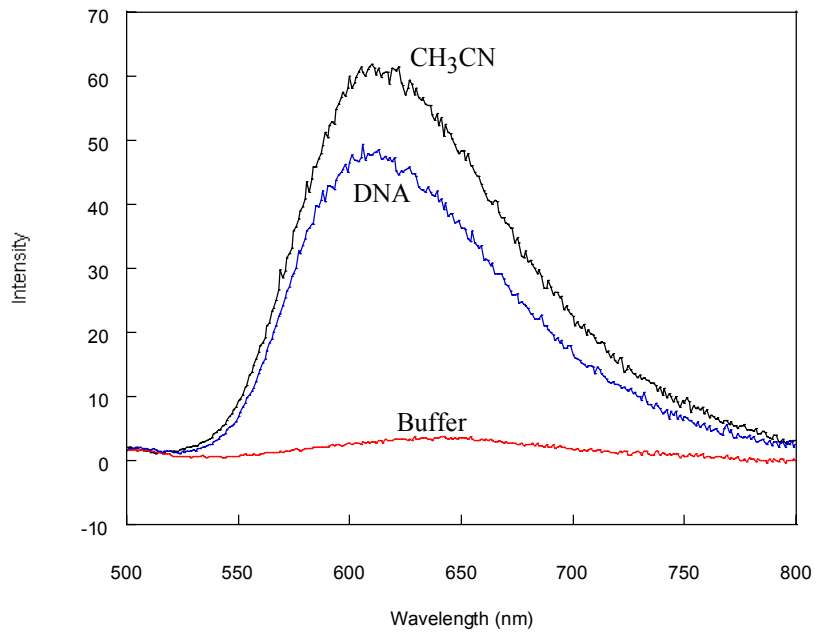

Figure 5.7 Fluorescence spectra of 10 μM $[Ru(5,5'\text{-}F_2bpy)_2dppz]^{2+}$ in the presence of acetonitrile, buffer of 5 mM NaPi, 50 mM NaCl, pH=7, and 1 mM calf thymus DNA. Excitation at 430 nm. Peak positions and quantum yields are listed in Table 5.4.

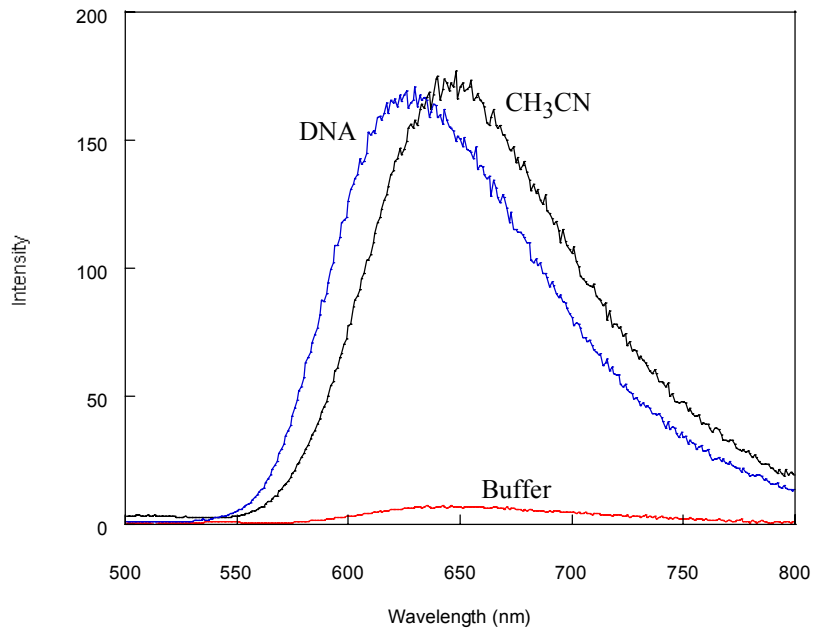

Figure 5.8 Fluorescence spectra of 10 μM $[Ru(4,4'\text{-}CHObpy)_2dppz]^{2+}$ in the presence of acetonitrile, buffer of 5 mM NaPi, 50 mM NaCl, pH=7, and 1 mM calf thymus DNA. Excitation at 458 nm. Peak positions and quantum yields are listed in Table 5.4.

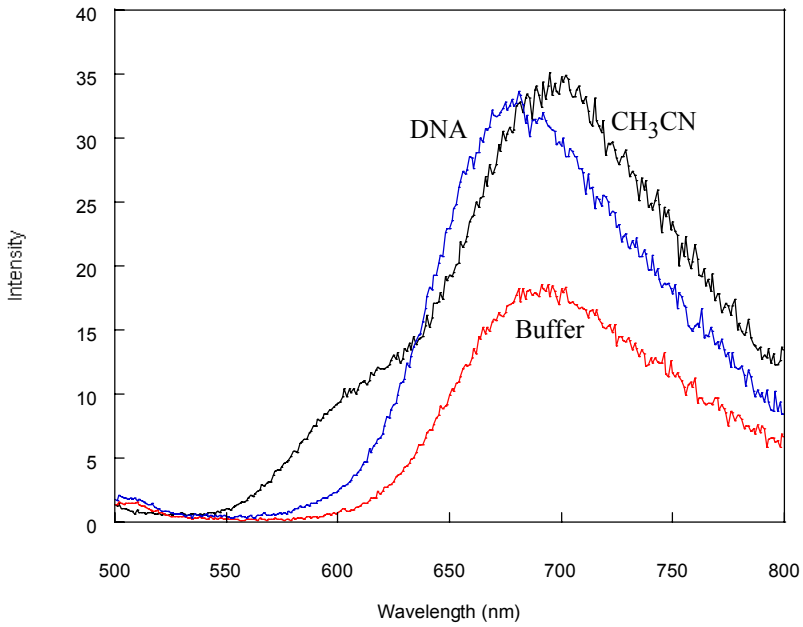

Figure 5.9 Fluorescence spectra of 10 μM $[Ru(5,5'\text{-}CF_3bpy)(phen)dppz]^{2+}$ in the presence of acetonitrile, buffer of 5 mM NaPi, 50 mM NaCl, pH=7, and 1 mM calf thymus DNA. Excitation at 430 nm. Peak positions and quantum yields are listed in Table 5.4.

	CH_3CN		Buffer		DNA	
Intercalator	ϕ	λmax	ϕ	λmax	ϕ	λmax
$[Ru(4,4'\text{-}CF_3bpy)_2dppz]^{2+}$	1.07	653 nm	0.90	646 nm	1.62	642 nm
$[Ru(5,5'\text{-}CF_3bpy)_2dppz]^{2+}$	0.23	672 nm	0.16	656 nm	0.21	656 nm
$[Ru(5,5'\text{-}F_2bpy)_2dppz]^{2+}$	0.17	610 nm	0.01	640 nm	0.13	608 nm
$[Ru(4,4'\text{-}CHObpy)_2dppz]^{2+}$	0.47	648 nm	0.02	645 nm	0.46	630 nm
$[Ru(5,5'\text{-}CF_3bpy)(phen)dppz]^{2+}$	0.11	700 nm	0.05	690 nm	0.09	680 nm

Table 5.4 Fluorescence parameters for the various intercalators in acetonitrile, buffer of 5 mM NaPi, 50 mM NaCl, pH=7, and 1 mM calf thymus DNA. Metal complex concentration in all cases was 10 μM. Excitation wavelength for each complex was at its respective MLCT maximum. Quantum yields are relative to a ruthenium(II) tris(bipyridine) in H_2O standard.

Luminescence Properties in Buffer +/- DNA. As shown in Table 5.4, the luminescence properties of the complexes differ greatly across the series in buffer and in buffer versus DNA. In buffer in the absence of DNA, dppz-based Ru(II) complexes are expected to show typical "light switch" behavior, in which little or no emission is detected relative to the same complex in the presence of DNA. This is what we observe for the complexes with 5,5'-F_2bpy and 4,4'-CHObpy as ancillary ligands. (The minor amount of emission with these complexes may be due to impurities unable to be removed via HPLC or because of reasons discussed below.) However, bipyridine ligands bearing trifluoromethyl substituents give rise to dppz-based complexes that fluoresce in aqueous solution. This suggests that the MLCT excited state of those complexes is not centered on the dppz ligand but rather on the ancillary bipyridine ligands. The altered electronic

structure created by the electron-withdrawing trifluoromethyl groups is obviously the reason for this.

In the presence of calf thymus DNA, all the metallointercalators exhibit enhanced fluorescence compared to free in a buffer solution. Similar to the results from studies in acetonitrile, electron-withdrawing substituents at the 4 and 4' positions give rise to greater quantum yields than those with electron-withdrawing groups at the 5 and 5' positions. The emission enhancements upon DNA binding are much smaller than observed for "normal" dppz-based ruthenium(II) polypyridyl intercalators,[1] supporting the UV-visible titration data that suggest the dppz ligand is not intercalated deeply into the helix because of unfavorable steric interactions.

Time-resolved fluorescence. Table 5.5 shows the excited-state lifetimes of the complexes in the presence of acetonitrile, buffer, and calf thymus DNA. In both acetonitrile and buffer, the observed excited-state lifetimes again correlate with the presence of electron-withdrawing groups at the 4 and 4' as opposed to the 5 and 5' positions on the bipyridine ligands. The reason for the relatively short lifetime of $[Ru(5,5'\text{-}CF_3bpy)(phen)dppz]^{2+}$ is unclear. Nevertheless, the data are consistent with a picture in which (at least some of) the MLCT excited state is localized on the bipyridine ligands.

In the presence of calf thymus DNA, the observed emission decays are best fit to a biexponential function, consistent with ruthenium(II) polypyridyl binding to the DNA double helix.[35] The longer-lived component of the lifetimes is larger than the corresponding lifetime in buffer, indicative of intimate interaction of the metal complex and the DNA helix. Once again, $[Ru(5,5'\text{-}CF_3bpy)(phen)dppz]^{2+}$ seems to be an aberration, as the percentage of the long-lifetime component for this complex in the presence of DNA is essentially zero. The binding of the complex to DNA is poor under the conditions used for the spectroscopy experiments.

Intercalator	CH_3CN τ	Buffer τ	DNA τ_1	DNA τ_2
$[Ru(4,4'\text{-}CF_3bpy)_2dppz]^{2+}$	324 ns	357 ns	130 ns (27%)	571 ns (73%)
$[Ru(5,5'\text{-}CF_3bpy)_2dppz]^{2+}$	148 ns	106 ns	121 ns (79%)	246 ns (21%)
$[Ru(5,5'\text{-}F_2bpy)_2dppz]^{2+}$	128 ns	162 ns	85 ns (71%)	372 ns (29%)
$[Ru(4,4'\text{-}CHObpy)_2dppz]^{2+}$	292 ns	443 ns	101 ns (60%)	481 ns (40%)
$[Ru(5,5'\text{-}CF_3bpy)(phen)dppz]^{2+}$	85 ns	49 ns	81 ns (98%)	274 ns (2%)

Table 5.5 Excited-state lifetimes for the various intercalators in acetonitrile, buffer of 5 mM NaPi, 50 mM NaCl, pH=7, and 1 mM calf thymus DNA. Racemic mixtures were used in all instances. Metal complex concentration in all samples was 10 μM. Excitation wavelength for each complex was at 470 nm. Observation wavelength was at the fluorescence maximum (as given in Table 5.4) for each sample.

5.3.4 Reactivity in the presence of DNA

Luminescence Quenching. The luminescence quenching of the metal complexes by ruthenium(III) hexaammine when bound to calf thymus DNA was systematically examined. Figure 5.10 shows Stern-Volmer plots for each of the quenching titrations. Complexes containing CF_3-modified bipyridines are quenched rather poorly relative to the CHO- and F-modified complexes. Quenching is most efficient with complexes whose excited states are localized on the intercalating dppz ligand.

Polyacrylamide Gel Electrophoresis (PAGE). Oxidative damage to DNA is generated with these complexes through a flash-quench experiment. *In situ* generated Ru(III) intercalators damage DNA via charge transfer to guanine followed by irreversible

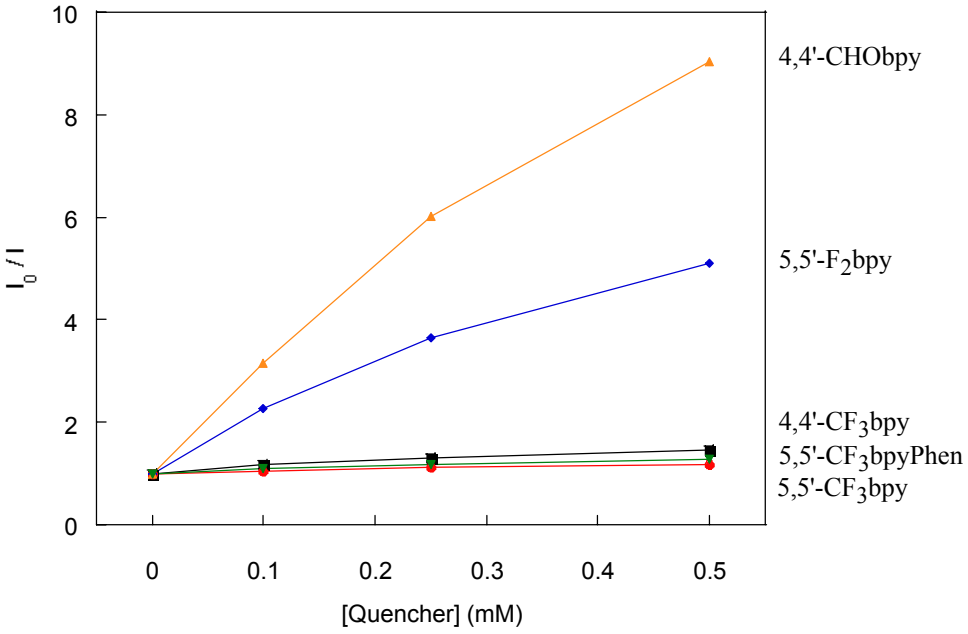

Figure 5.10 Stern-Volmer quenching plots for the quenching of 10 μM Ru by ruthenium(III) hexaammine in 1 mM calf thymus DNA in 5 mM NaPi, 50 mM NaCl, pH=7 buffer. Excitation for each complex was at its respective MLCT maximum (see Table 5.1) and fluorescence intensities were integrated from 500–800 nm.

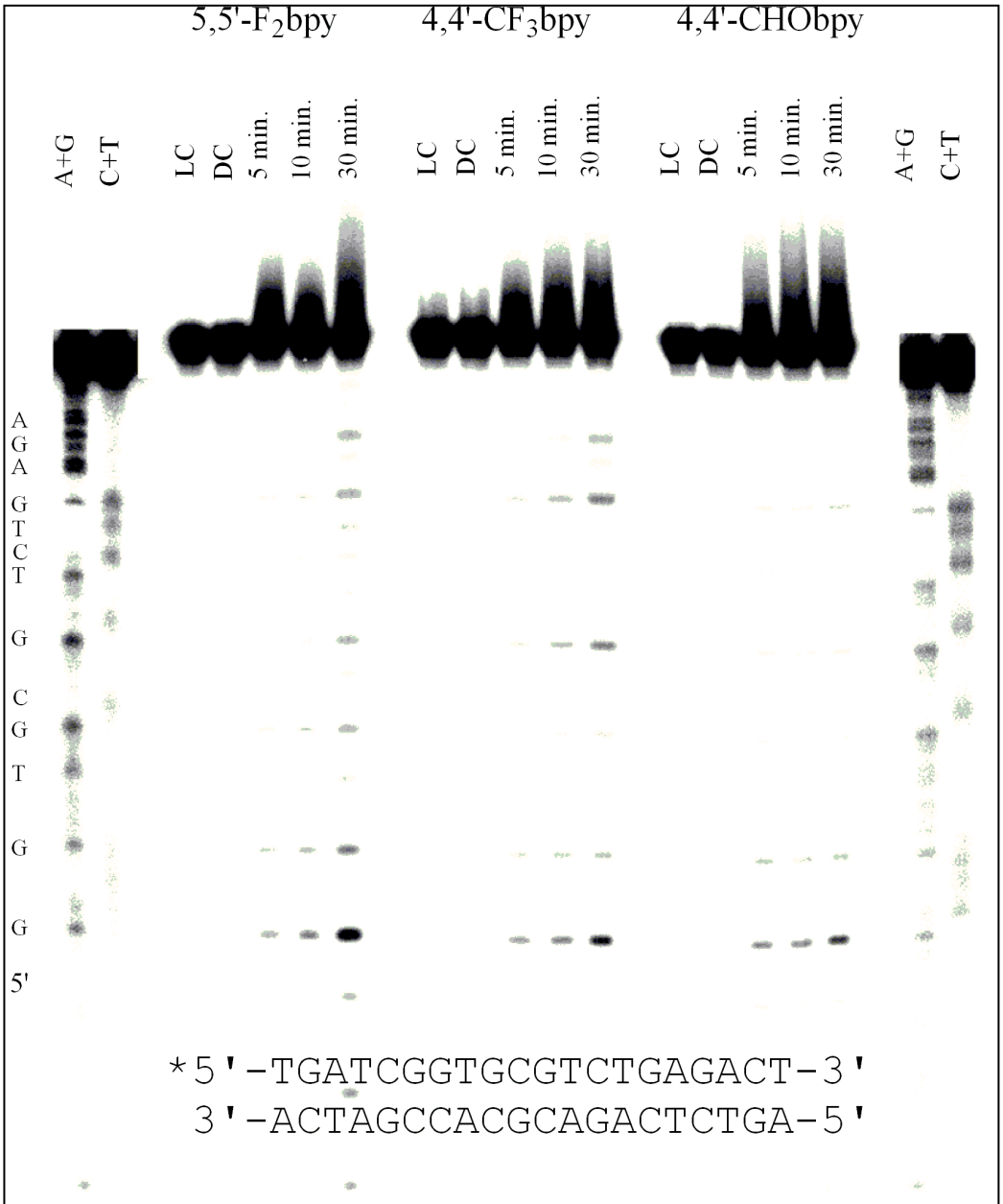

Figure 5.11 Gel demonstrating oxidative damage to DNA via the flash-quench technique. Shown at the bottom is the sequence of the DNA used for electrophoresis experiments (site of ^{32}P labelling indicated by *). LC = Light control (no quencher). DC = Dark control (no irradiation). Irradition times at 450 nm given in minutes. Outside lanes on each side of the gel are Maxam-Gilbert sequencing reactions. Samples contain 16 μM metal complex, 8 μM DNA, and 160 μM $Ru(NH_3)_6^{3+}$. Buffer in all samples is 5 mM NaPi, 50 mM NaCl, pH=7.

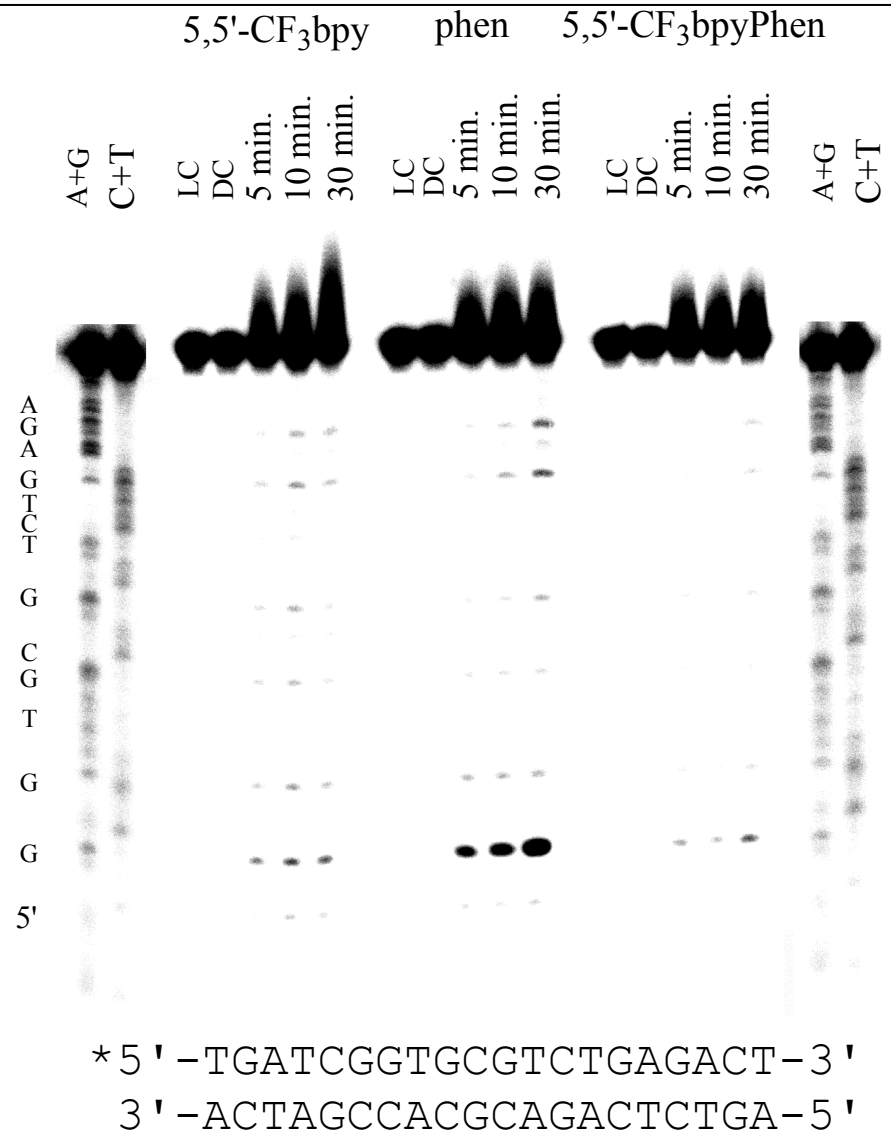

Figure 5.12 Gel demonstrating oxidative damage to DNA via the flash-quench technique. Shown at the bottom is the sequence of the DNA used for electrophoresis experiments (site of ^{32}P labelling indicated by *). LC = Light control (no quencher). DC = Dark control (no irradiation). Irradition times at 450 nm given in minutes. Outside lanes on each side of the gel are Maxam-Gilbert sequencing reactions. Samples contain 16 μM metal complex, 8 μM DNA, and 160 μM $Ru(NH_3)_6^{3+}$. Buffer in all samples is 5 mM NaPi, 50 mM NaCl, pH=7.

chemistry taking place at the guanine radical site.[36,37] Figures 5.11 and 5.12 show the PAGE analysis for the oxidation of guanine in duplex DNA by the series of dppz-based ruthenium intercalators with varying oxidation potentials. As expected, the predominant amount of damage occurs at the 5'-G of a 5'-GG-3' doublet on the radioactively labeled strand. This site specificity is consistent with charge transfer and rules out singlet oxygen damage as a major contributor to guanine oxidation. For all metal complexes, increasing the irradiation time increases the amount of damage observed. Importantly, however, the yields of oxidation do not correlate with increasing oxidation potential. The metal complex with the lowest 3+/2+ potential, $[Ru(phen)_2dppz]^{2+}$, yields the greatest amount of damage. Other factors must play a role in determining how the intercalator reacts chemically with the DNA. The results do correlate, however, with how well the excited state of the metal complex is quenched (and therefore how much Ru(III) is produced *in situ*). Stacking, oxidation potential, and quenching efficiency all play a major role in this reaction. Therefore, one must be careful in analyzing data based on one of these parameters alone.[32]

EPR. The flash-quench technique has also been used to generate guanine radicals in DNA which can be observed by EPR spectroscopy.[16] Given the high oxidation potentials of the ruthenium complexes synthesized for these studies, it is not unreasonable to ask if they are able to oxidize bases in DNA other than guanine. Adenine[9] and the base analog inosine[38] are the next easiest to oxidize in DNA, so high oxidation potentials may be able to generate adenine or inosine radicals in DNA that can be observed via EPR spectroscopy.

EPR experiments were carried out by irradiating selected metal complexes in the presence of a sacrificial quencher (cobalt(III) pentaammine chloride) and the DNA polymers poly d(GC), poly d(AT), and poly d(IC). The signals observed are shown in Figures 5.13–5.15.

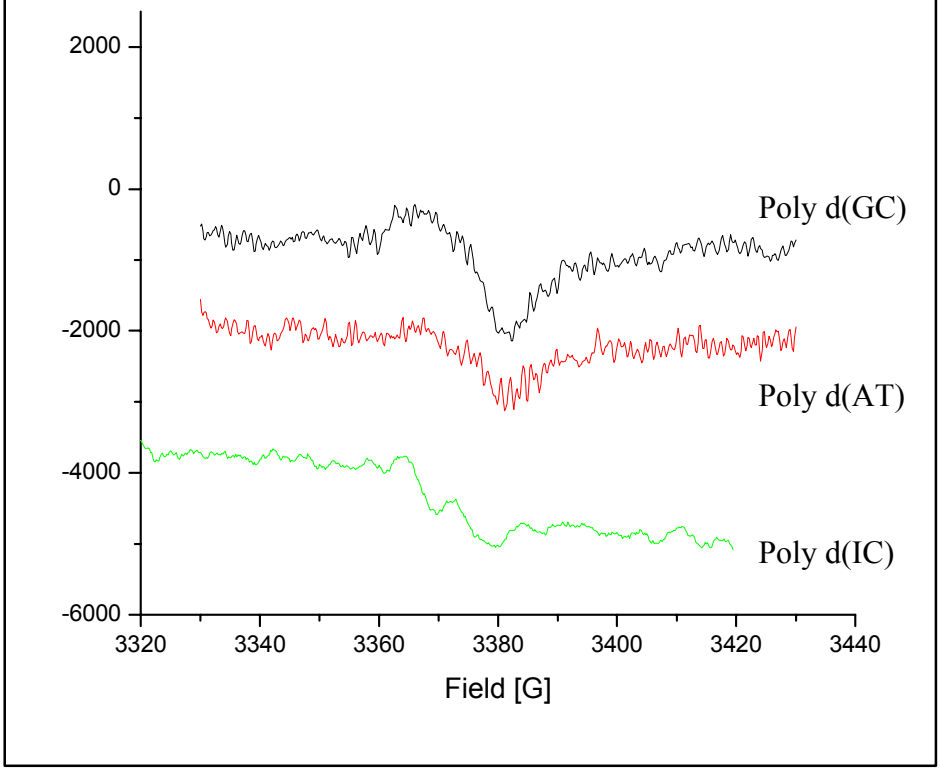

Figure 5.13 EPR signals of frozen samples (77 K) obtained by irradiating 20 μM $[Ru(5,5'\text{-}CF_3bpy)_2dppz]^{2+}$ in the presence of 0.4 mM cobalt(III) pentaammine chloride and 0.8 mM nucleotides of various DNA polymers. Irradiation carried out with a 300W Xe arc lamp with filters employed to eliminate $\lambda<320$ nm light. Buffer in all samples was 10 mM KPi, 10 mM NaCl, pH=7.

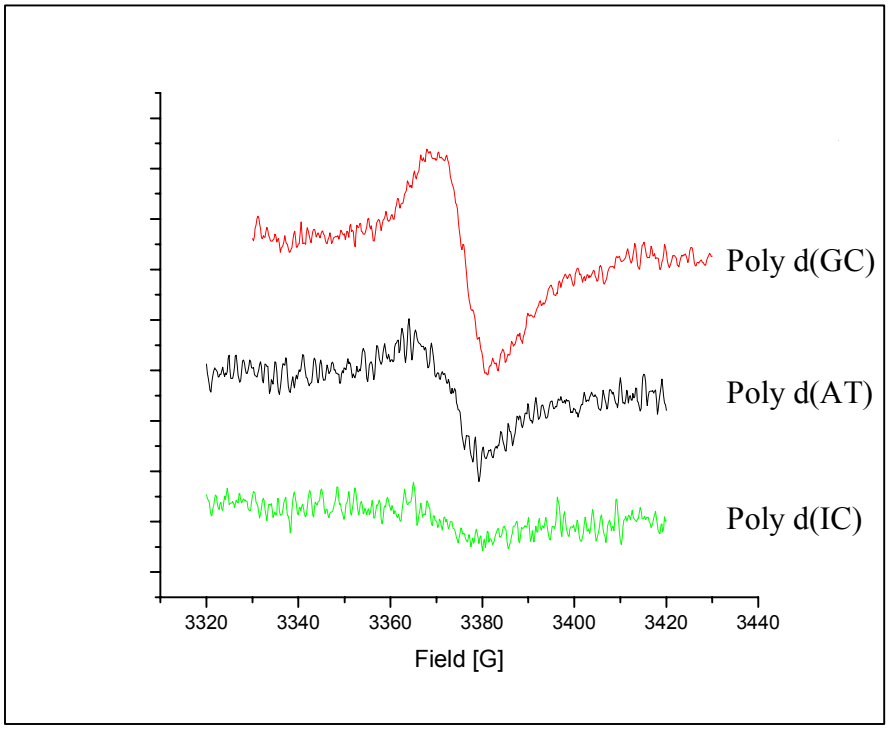

Figure 5.14 EPR signals of frozen samples (77 K) obtained by irradiating 20 μM $[Ru(5,5'\text{-}F_2bpy)_2dppz]^{2+}$ in the presence of 0.4 mM cobalt(III) pentaammine chloride and 0.8 mM nucleotides of various DNA polymers. Irradiation carried out with a 300W Xe arc lamp with filters employed to eliminate $\lambda<320$ nm light. Buffer in all samples was 10 mM KPi, 10 mM NaCl, pH=7.

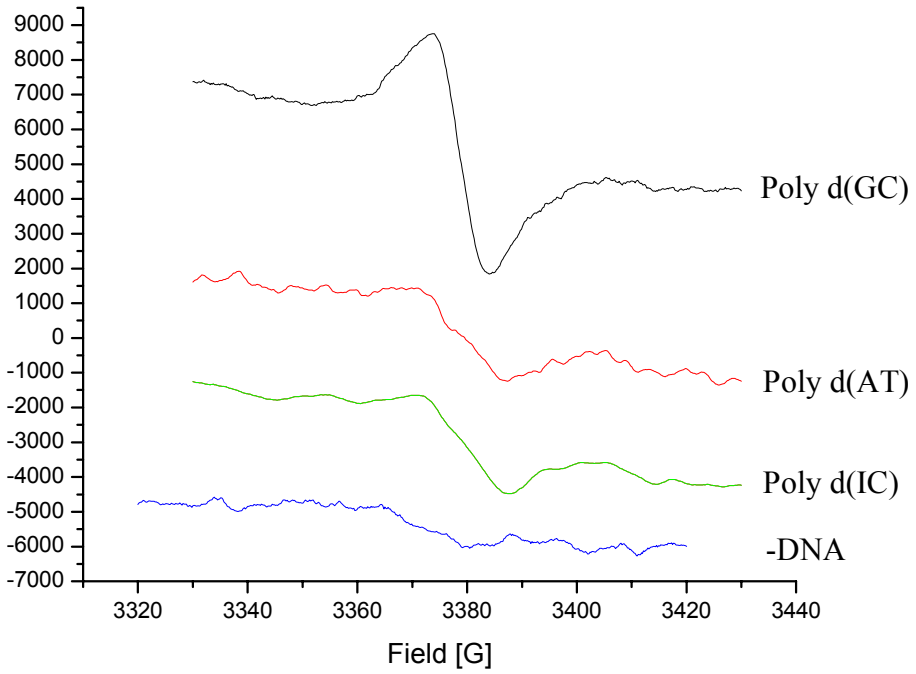

Figure 5.15 EPR signals of frozen samples (77 K) obtained by irradiating 20 μM $[Ru(4,4'\text{-}CHObpy)_2dppz]^{2+}$ in the presence of 0.4 mM cobalt(III) pentaammine chloride and 0.8 mM nucleotides of various DNA polymers. Irradiation carried out with a 300W Xe arc lamp with filters employed to eliminate $\lambda<320$ nm light. Buffer in all samples was 10 mM KPi, 10 mM NaCl, pH=7.

$[Ru(5,5'\text{-}CF_3bpy)_2dppz]^{3+}$ (Figure 5.13) and $[Ru(5,5'\text{-}F_2bpy)_2dppz]^{3+}$ (Figure 5.14) give rise to small EPR signals in the presence of poly d(GC) and poly d(AT). The signals in the presence of poly d(IC) are negligible. $[Ru(4,4'\text{-}CHObpy)_2dppz]^{3+}$ (Figure 5.15) readily oxidizes guanine in poly d(GC), as is apparent from the large EPR signal obtained in the presence of that polymer. Interestingly, a small signal is also observed for poly d(AT) and poly d(IC). A small amount of adenine and inosine are also being oxidized. It should also be noted that there is a tiny signal in the absence of DNA; this could be indicative of impurities in the metal complex or the buffer. Notably, the signal sizes observed correlate directly with the amount of *in situ* Ru(III), as determined from steady-state luminescence quenching values. The specific signals in various polymers and the signal sizes do not correlate with oxidation potential. Thus, we must be careful and consider our results (*vide supra*) that indicated energetics is not the sole factor in determining reactivity with DNA.

Transient Absorption Spectroscopy. Time-resolved transient absorption spectroscopy has also been used to observe guanine radicals created via a flash-quench cycle in DNA.[15] We employed this technique to study the systems described in the EPR section (*vide supra*) in the hopes of seeing long-lived spectroscopic signals indicative of DNA base radical formation. Figures 5.16–5.18 illustrate the transient absorption spectra of the ruthenium dppz-based intercalators in the presence of polynucleotides and quencher. The excited state of the complexes in the absence of quencher is also shown. In no case is a long-lived signal observed. Other wavelengths were probed and yielded similar results. This was not surprising, because the quenching efficiency is very poor. Any small amount of radical signal generated would be hidden under the large signal from the ruthenium(II) excited state. Also, a major difference between the EPR and transient absorption experiments is that the EPR data were collected under low-temperature (77 K) conditions. This low temperature during the EPR experiments could allow the radicals to live longer and be observed under those reaction conditions.

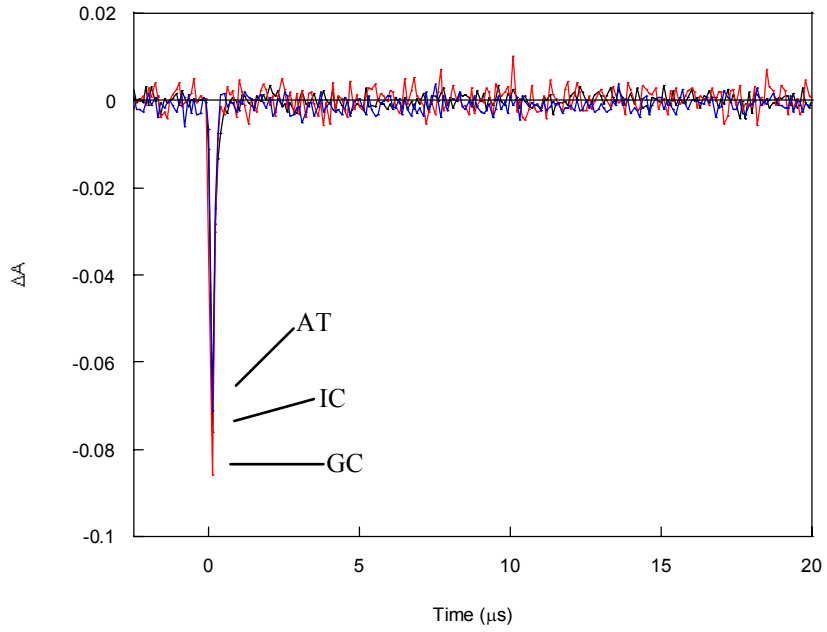

Figure 5.16 Transient absorption at 440 nm obtained by irradiating 20 μM $[Ru(5,5'\text{-}CF_3bpy)_2dppz]^{2+}$ with various DNA polymers in the presence of 0.4 mM ruthenium(III) hexaammine in 5 mM NaPi, 50 mM NaCl, pH=7. Spectra recorded at ambient temperature (ca. 294 K) with λ_{exc}=470 nm and [DNA] = 1 mM.

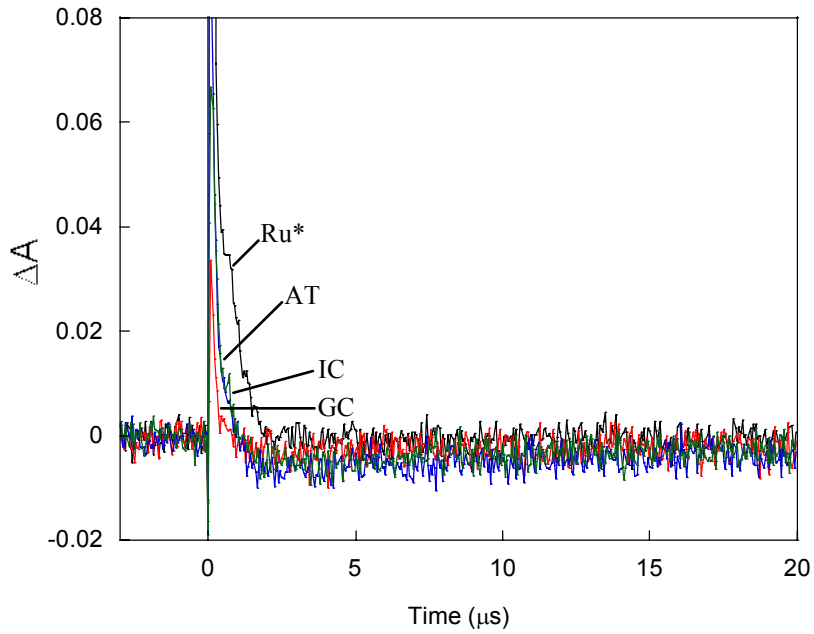

Figure 5.17 Transient absorption at 440 nm obtained by irradiating 20 μM $[Ru(5,5'\text{-}F_2bpy)_2dppz]^{2+}$ with various DNA polymers in the absence and presence of 0.4 mM ruthenium(III) hexaammine in 5 mM NaPi, 50 mM NaCl, pH=7. Spectra recorded at ambient temperature (ca. 294 K) with λ_{exc}=470 nm and [DNA] = 1 mM.

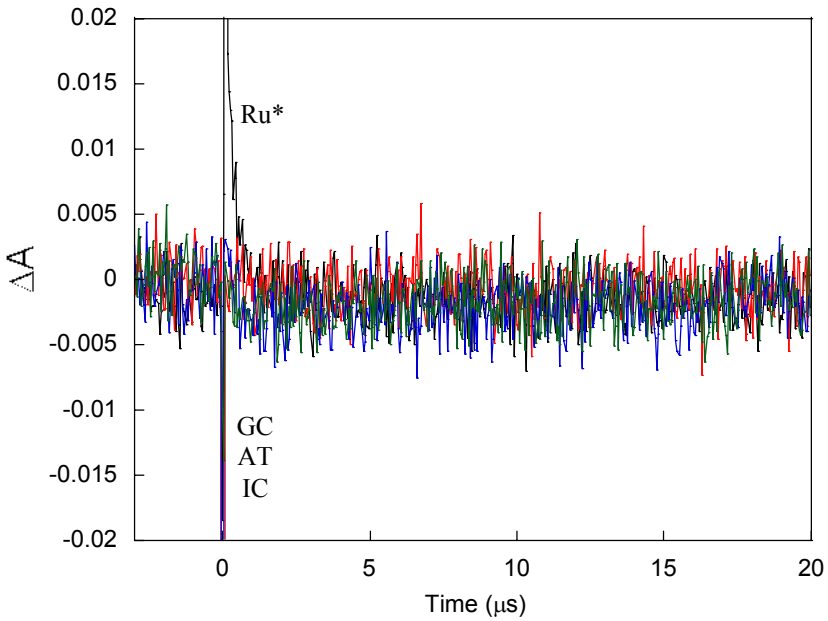

Figure 5.18 Transient absorption at 440 nm obtained by irradiating 20 μM $[Ru(4,4'\text{-}CHObpy)_2dppz]^{2+}$ with various DNA polymers in the absence and presence of 0.4 mM ruthenium(III) hexaammine in 5 mM NaPi, 50 mM NaCl, pH=7. Spectra recorded at ambient temperature (ca. 294 K) with λ_{exc}=470 nm and [DNA] = 1 mM.

5.4 Discussion

5.4.1 Redox properties

The synthesis and characterization of a wide range of ruthenium(II) polypyridyl intercalators have allowed us to develop an adequate description of the electronic structure of these complexes. Electron-withdrawing substituents on the ancillary (non-intercalating) 2,2'-bipyridine ligands increase the oxidation potential of the compounds up to +0.2 V relative to their unmodified counterparts. The observed oxidation potentials (+1.66 to +1.84 V) correlate with the electron-withdrawing ability of the substituents on the bpy ligands. The greater the electron-withdrawing-ability of the substituents on the bpy ligands, the higher the oxidation potential of the metal complex.

5.4.2 Spectroscopic properties in the absence of DNA

UV-visible Spectroscopy. The UV-visible spectra of the complexes in water are typical of ruthenium(II) polypyridyl compounds. The broad metal-to-ligand charge transfer band is present for all complexes in the 400–500 nm regime, in agreement with other dipyridophenazine-based ruthenium intercalators.[1] UV-visible data alone are insufficient to describe the MLCT excited state as localized on one of the ligands. Unlike other intercalators, the energy of the dppz π-π^* transition is affected by the ancillary ligands. More electron-withdrawing groups shift the π-π^* band to higher energy, suggesting modified ligands alter the electronic coupling between the dppz and the metal center. As expected, bpy π-π^* transitions also appear in the ultraviolet region of the spectrum.

Emission Spectroscopy. Steady-state spectroscopy reveals clues to the exact nature of the MLCT excited state in these complexes. The luminescence properties of the complexes in acetonitrile depend on whether the ancillary bipyridines are substituted at the 4 and 4' or 5 and 5' positions. Higher quantum yields observed for metal complexes with 4,4' substituted bpy ligands is consistent with those positions stabilizing the excited (emissive) state of Ru(II).

The fluorescence behavior in buffer, however, is quite different. Typical dppz-based Ru(II) intercalators show no luminescence in aqueous solution because their emission is quenched by proton interaction with the phenazine nitrogens on the dppz. The complexes we studied that incorporate trifluoromethyl groups on the bpy ancillary ligands exhibit moderate emission in buffer solution (Table 5.4). The most likely explanation for this anomaly is that the electron-withdrawing substituents have altered the excited state of the metal complex so that it is localized on the bipyridine (bpy) units instead of the dipyridophenazine. The MLCT localized on the modified bpy ligands is not as susceptible to quenching via proton transfer or hydrogen bonding like the dppz-based MLCT,[4,5] hence luminescence quenching of the excited state is not as rapid and the complexes emit in aqueous solution.

5.4.3 Spectroscopic properties in the presence of DNA

UV-visible Spectroscopy. The binding of the metal complexes to DNA was examined by monitoring the spectroscopically distinct π-π^* absorption transition of the dppz moiety. Hypochromism as a result of DNA intercalation of the dppz was observed for all of the complexes we studied (Table 5.3). The extent of hypochromism, however, was much lower than the values typically observed for dppz-based intercalators. The effect was especially pronounced when substituents were located at the 5 and 5' position on the ancillary bipyridine ligands. At these positions the substituents could sterically clash with the helix when bound to DNA. These unfavorable interactions would prevent deep intercalation of the dppz into the double helix. This is manifested in small hypochromism percentages upon binding to DNA.

Steady-state Emission Spectroscopy. The luminescence behavior of the series of complexes in the presence of DNA was also investigated. Addition of DNA to buffer solutions containing metal complex results in increased emission of the ruthenium excited state. Emission enhancement is most pronounced for the F- and CHO-substituted bpy containing complexes. In those complexes, the MLCT is localized primarily on the

dppz ligand, and intercalation into DNA protects the dppz from quenching by protons in solution. While the other complexes show emission enhancements, the effect is not as great in those cases because the MLCT is not centered on the dppz ligand. For all complexes, the quantum yield is higher if the electron-withdrawing substituents are located at the 4 and 4' positions of the bpy ligand. This is again consistent with those positions giving rise to electronic stabilization of the ruthenium excited state.

Time-resolved Fluorescence Spectroscopy. Time-resolved measurements reveal a biexponential decay for the excited state of the ruthenium complexes when bound to DNA. The longer component of the decay is slower than corresponding excited-state decay in water or DNA for all of the complexes we studied. This is indicative of intimate interaction of the metal complexes with the DNA double helix. The value of this long component correlates, once again, with the presence of substituents at the 4 and 4' versus the 5 and 5' positions on the bpy ligands. This reinforces the idea that 4 and 4' electron-withdrawing-substituents stabilize the ruthenium excited state. It does not, however, take into account that the reason for shorter lifetimes in the 5 and 5' substituted bpy complexes could also be a result of steric interactions with the DNA which decrease their affinity for the double helix.

5.4.4 Reactivity with DNA

Luminescence Quenching. We used the electron-accepting quencher ruthenium(III) hexaammine to examine luminescence quenching of the ruthenium(II) excited states of the various complexes when bound to DNA. Complexes containing CF_3-modified bipyridines are quenched rather poorly relative to the CHO- and F-modified complexes. This correlates with the location of the MLCT excited state. When CF_3-modified bipyridines are present, the MLCT funnels electron density to the ancillary ligands rather than the intercalating dppz ligand, and the quenching is poor. The trend is exactly opposite of what we would expect, because the excited state localized on the ancillary ligands should be more accessible to quencher. The excited states should have

enough thermodynamic driving force to react with the quencher in all cases, so unfavorable energetics may be ruled out as a contributing factor. UV-visible hypochromism data indicate the complexes are not bound well to the DNA anion, a result of unfavorable steric interactions between the trifluoromethyl groups and the DNA sugar-phosphate backbone. This would decrease the likelihood of a van der Waals contact reaction with the positively charged ruthenium(III) hexaammine and give lower quenching yields. It is important to keep this quenching behavior in mind when examining the chemistry of these complexes with DNA.

Oxidative damage to DNA. The flash-quench technique and polyacrylamide gel electrophoresis were employed to examine guanine damage in a short DNA duplex. The damage at the 5'-G of a 5'-GG-3' site was monitored for the various modified intercalators over a series of reaction times. The amount of oxidative damage observed at the guanine doublet did not correlate directly with the oxidation potential of the ruthenium intercalators. The 5,5'-CF_3bpy (+1.84 V) and 4,4'-CF_3bpy (+1.80 V) containing complexes induced only small amounts of damage even though they possess the highest oxidation potentials. The amount of damage did correlate, however, with the luminescence quenching yields as measured in calf thymus DNA with a ruthenium(III) hexaammine quencher. This indicates that once the intercalators have sufficient oxidation potential to oxidize guanines, the amount of Ru(III) generated *in situ* has more of an effect on the amount of damage to DNA than does small increases in the oxidation potential. Binding affinity also plays a significant role, and steric clashes of the trifluoromethyl group with the DNA backbone could play a large part in the reduced reactivity of CF_3-substituted bpy compounds with DNA.

EPR and Transient Absorption Spectroscopy. The flash-quench technique was also used in conjunction with electron paramagnetic resonance and transient absorption spectroscopy in attempts to observe radicals in DNA generated by various dppz-based intercalators. Signals indicative of purine base radicals were observed in the presence of

both poly d(GC) and poly d(AT) for $[Ru(5,5\text{-}CF_3bpy)_2dppz]^{3+}$, $[Ru(5,5,\text{-}F_2bpy)_2dppz]^{3+}$, and $[Ru(4,4'\text{-}CHObpy)_2dppz]^{3+}$. A signal was also observed in the presence of poly d(IC) with $[Ru(4,4'\text{-}CHObpy)_2dppz]^{3+}$. Once again, the signals correlated with the amount of *in situ* generated Ru(III) but not the absolute oxidation potential of the metal complex. It should be noted, however, that the EPR experiments were performed at low temperature (77 K) and with a sacrificial quencher. These conditions could increase the lifetime of the DNA base radicals and allow them to be seen with metal complexes and DNA polymers even though they may not be observed under more "normal" conditions.

Transient absorption spectroscopy was performed on the same metal complexes and DNA polymers as examined in the EPR experiments. These studies, though, required that ambient temperatures be used. The spectra revealed no long-lived signals corresponding to DNA base radicals under these conditions. This was not surprising, because the ruthenium(II) excited state of the complexes is poorly quenched by $[Ru(NH_3)_6]^{3+}$. The spectra were simply the decay of the ruthenium excited state. Even if base radicals were generated, they would have been extremely difficult to observe.

5.5 Conclusions

Modification of ancillary 2,2'-bipyridine ligands gave a series of dppz-based ruthenium(II) intercalators with a wide range of redox potentials, spectral properties, and DNA reactivity. Overall, the chemistry of the modified intercalators with DNA is dependent upon a number of factors. While oxidation potential is important in determining whether or not a given intercalator will react with the DNA base stack, it is clearly not the sole predictor in determining the extent of that reactivity. The most important factors are (1) how well the intercalators are stacked and thus electronically coupled to the DNA double helix and (2) how efficiently the excited state is quenched to generate the reactive Ru(III) species. An interplay of these factors with oxidation potential is what gives rise to the reactive behavior observed with DNA.

5.6 References

1. (a) Friedman, A. E.; Chambron, J.-C.; Sauvage, J.-P.; Turro, N. J.; Barton, J. K. *J. Am. Chem. Soc.* **1990**, *112*, 4960. (b) Jenkins, Y.; Friedman, A. E.; Turro, N. J.; Barton, J. K. *Biochemistry* **1992**, *32*, 10809.

2. (a) Dupureur, C. M.; Barton, J. K. *J. Am. Chem. Soc.* **1994**, *116*, 10286. (b) Dupureur, C. M.; Barton, J. K. *Inorg. Chem.* **1997**, *36*, 33.

3. Holmlin, R. E.; Stemp, E. D. A.; Barton, J. K. *Inorg. Chem.* **1998**, *37*, 29.

4. Turro, C.; Bossman, S. H.; Jenkins, Y.; Barton, J. K.; Turro, N. J. *J. Am. Chem. Soc.* **1995**, *117*, 9026.

5. Olson, E. J. C.; Hu, D.; Hormann, A.; Jonkman, A. M.; Arkin, M. R.; Stemp, E. D. A.; Barton, J. K.; Barbara, P. F. *J. Am. Chem. Soc.* **1997**, *119*, 11458.

6. Holmlin, R. E.; Dandliker, P. J.; Barton, J. K. *Angew. Chem. Int. Ed. Engl.* **1997**, *36* 2715.

7. Schuster, G. B. *Acc. Chem. Res.* **2000**, *33*, 253.

8. Núñez, M. E.; Noyes, K. T.; Gianolio, D. A.; McLaughlin, L. W.; Barton, J. K. *Biochemistry* **2000**, *39*, 6190.

9. Steenken, S.; Jovanovic, S. V. *J. Am. Chem. Soc.* **1997**, *119*, 617.

10. (a) Sugiyama, H.;Saito, I. *J. Am. Chem. Soc.* **1996**, *118*, 7063. (b) Prat, F.; Houk, K. N.; Foote, C. S. *J. Am. Chem. Soc.* **1998**, *120*, 845.

11. Arkin, M. R.; Stemp, E. D. A.; Pulver, S. C.; Barton, J. K. *Chem. Biol.* **1997**, *4*, 389.

12. Núñez, M. E.; Hall, D. B.; Barton, J. K. *Chem. Biol.* **1999**, *6*, 85.

13. Núñez, M. E.; Noyes, K. T.; Barton, J. K. *Chem. Biol.* **2002**, *9*, 403.

14. Chiang, I.-J.; Gray, H. B.; Winkler, J. R. *J. Am. Chem. Soc.* **1991**, *113*, 3621.

15. Stemp, E. D. A.; Arkin, M. R.; Barton, J. K. *J. Am. Chem. Soc.* **1997**, *119*, 2921.

16. Schiemann, O.; Turro, N. J.; Barton, J. K. *J. Phys. Chem. B.* **2000**, *104*, 7214.

17. Hartshorn, R. M.; Barton, J. K. *J. Am. Chem. Soc.* **1997**, *119*, 2921.

18. Holmlin, R. E.; Yao, J. A.; Barton, J. K. *Inorg. Chem.* **1999**, *38*, 174.

19. Lever, A. B. P. *Inorg. Chem.* **1990**, *29*, 1271.

20. Dickeson, J. E.; Summers, L. A. *Aust. J. Chem.* **1970**, *23*, 1023.

21. Waterland, M. R.; Gordon, K C.; McGarvey, J. M; Jayaweera, P. M. *J. Chem. Soc., Dalton Trans.* **1998**, 609.

22. Chan, K. S., Tse, A. K. S. *Synth. Comm.* **1993**, *23*, 1929.

23. Furue, M.; Maruyama, K.; Oguni, T.; Naiki, M.; Kamachi, M. *Inorg. Chem*. **1992**, *31*, 3792.

24. Sullivan, B. P.; Salmon, D. J.; Meyer, T. J. *Inorg. Chem.* **1978**, *17*, 3334.

25. Amouyal, E.; Homsi, A.; Chambron, J.-C.; Sauvage, J.-P. *J. Chem. Soc., Dalton Trans.* **1990**, 1841.

26. Anderson, P. A.; Deacon, G. B.; Haarmann, K. H.; Keene, F. R.; Meyer, T. J.; Reitsma, D. A.; Skelton, B. W.; Strouse, G. F.; Thomas, N. C.; Treadway, J. A.; White, A. H. *Inorg. Chem*. **1995**, *34*, 6145.

27. St. C. Black, D.; Deacon, G. B.; Thomas, N. C. *Aust. J. Chem.* **1982**, *35*, 2445.

28. Thomas, N. C.; Deacon, G. B. *Inorg. Synth.* **1989**, *25*, 107.

29. Hand, E. S.; Baker, D. C. *Synthesis* **1989**, 905.

30. Cantor, C. R.; Warshaw, M. M.; Shapiro, H. *Biopolymers* **1970**, *9*, 1059.

31. Warshaw, M. M.; Tinoco, I. *J. Mol. Bio.* **1966**, *1*, 29.

32. Delaney, S.; Pascaly, M.; Bhattacharya, P. K.; Han, K.; Barton, J. K. *Inorg. Chem*. **2002**, *41*, 1966.

33. Hiort, C.; Lincoln, P.; Nordén, B. *J. Am. Chem. Soc.* **1993**, *115*, 3448.

34. Caspar, J. V.; Kober, E. M.; Sullivan, B. P.; Meyer, T. J. *J. Am. Chem. Soc.* **1982**, *104*, 630.

35. Kumar, C. V.; Barton, J. K.; Turro, N. J. *J. Am. Chem. Soc.* **1985**, *107*, 5518.

36. Burrows, C. J.; Muller, J. G. *Chem. Rev.* **1998**, *98*, 1109.

37. Angelov, D.; Spassky, A.; Berger, M.; Cadet, J. *J. Am. Chem. Soc.* **1997**, *119*, 11373.

38. Kelley, S. O.; Barton, J. K. *Science* **1999**, *283*, 375.